Journal of Extracellular Biology

RESEARCH ARTICLE OPEN ACCESS

Exosome Secretion Drives Chemo-Resistance of Temozolomide in Glioblastoma

Wenpei Li[1] | Shaoping Jiang[1] | Kun Liu[1] | Zhi Li[1] | Jun Yang[1] | Weimin Liu[1] | Yuanyu Huang[1,2,3,4] | Minghui Yang[1,2,3,4] | Shuai Guo[1,2] | Shaobo Ruan[1,2]

[1]School of Chemistry and Chemical Engineering, School of Life Science, School of Interdisciplinary Science, Key Laboratory of Molecular Medicine and Biotherapy, Key Laboratory of Medical Molecule Science and Pharmaceutics Engineering, Beijing Institute of Technology, Beijing, China | [2]School of Medical Engineering, School of Interdisciplinary Science; Affiliated Zhuhai People's Hospital, Beijing Institute of Technology, Zhuhai, P.R. China | [3]Advanced Technology Research Institute, Beijing Institute of Technology, Ji'nan, China | [4]Beijing Key Laboratory of Mucosal Immunity Vaccines Against Respiratory Viruses, Beijing Institute of Technology, Beijing, China

Correspondence: Shuai Guo (sguo@bit.edu.cn) | Shaobo Ruan (ruanshaobo@bit.edu.cn)

Received: 4 March 2026 | **Revised:** 31 May 2026 | **Accepted:** 3 June 2026

ABSTRACT

Temozolomide (TMZ) is a first-line chemotherapeutic agent for the treatment of glioblastoma (GBM), while a majority of patients do not effectively respond to TMZ owing to the multiple resistance mechanisms. In this study, we found that TMZ treatment substantially increased the exosome secretion from GBM cell line. The secreted exosomes from TMZ-treated C6 cells maintained typical physicochemical properties, with only slight fluctuation in expression profile of surface markers compared to untreated cell-derived exosomes. Further investigation revealed that increased expression of p53 might be the predominant reason to promote exosome secretion, potentially through the upregulation of six-transmembrane epithelial antigen of prostate 3 (STEAP3) expression under stress condition. Moreover, we identified that pre-treatment with TMZ-induced exosomes could reduce the sensitivity of C6 cells to TMZ and considered that exosome secretion may serve as a potent TMZ resistance mechanism via enhancing anti-apoptotic ability of GBM cells towards TMZ exposure. Proteomics analysis revealed a strategic mechanism to resist TMZ-induced apoptosis by upregulating exosomal proteins associated with biogenesis, chemoresistance, and therapeutic adaption. This finding revealed a considerable TMZ resistance mechanism and provided a new inspiration for preventing exosome biogenesis to resensitise TMZ cytotoxicity towards GBM.

1 | Introduction

Glioblastoma (GBM) is the most common and aggressive diffuse glioma of astrocytic lineage in adults, making up approximately 50% of all glioma and 15% of all primary brain tumours (Berenguer et al. 2018). GBM is classified into Grade IV glioma based on the WHO classification, characterised by high invasiveness, high recurrence rates, high mortality and poor prognosis (Dusoswa et al. 2019). Despite a standard treatment comprising maximal safe surgical resection, followed by concurrent radiation therapy and adjuvant chemotherapy, GBM remains incurable malignancy with a median survival of only 15 months (Wong et al. 2020). Temozolomide (TMZ), an oral alkylating agent, can transfer alkyl groups to guanine and adenine bases, inducing adducts accumulation and thus DNA damage (Yin et al. 2023). Since 2005, TMZ is considered as the first-line chemotherapeutic agent of GBM due to its comparatively superior blood–brain barrier (BBB) penetration efficiency. However, the survival benefits of TMZ treatment are still modest, with a 2.5 months improvement in the median survival from 12.1 to 14.6 months (Lee 2016). The modest survival benefit is mainly attributed to the existence of multiple resistance mechanisms, primarily including O-6-methyl guanine-

DNA methyltransferase (MGMT)-mediated double-strand DNA repair (Wu et al. 2019; Oldrini et al. 2020), poly-ADP-ribose polymerase (PARP)-mediated base excision repair (Han et al. 2020; Wu et al. 2021), P-glycoprotein (P-gp) efflux pump (Munoz et al. 2015; Robey et al. 2018), the presence of specific cell population such as glioma stem cells (GSCs) (Tso et al. 2015; Xu et al. 2024) and glioma-associated macrophage (GAM) (Broekman et al. 2018; Jiang et al. 2024), the accumulation of stress-survival responses (e.g., autophagy), as well as alteration in cell signalling pathway (e.g., PI3K/Akt). Therefore, understanding the underlying resistance mechanisms or uncovering new resistance mechanism may offer more opportunities to troubleshoot the TMZ resistance and improve survival benefit.

Extracellular vesicles (EVs) are lipid bilayer-enclosed membrane vesicles secreted from nearly all mammalian cell types and are broadly classified into three subtypes according to their origin and size: exosomes (30–150 nm), microvesicles (100–1000 nm) and apoptotic bodies (800–5000 nm) (Liu et al. 2019; Hussain et al. 2025). Among these, exosomes are the most widely studied EVs given to their well-defined endosomal origin, significant roles in intercellular communication by transferring bioactive cargo (e.g., proteins, miRNAs and metabolites) (Zhang et al. 2018; Yang et al. 2020; Kimiz-Gebologlu and Oncel 2022; Song et al. 2024), as well as their considerable potential in various biomedical applications (e.g., tissue repair, drug delivery and liquid biopsy) (Liang et al. 2021; Yu et al. 2022; Yadav et al. 2024). Briefly, exosomes are generally recognised to originate from the inward budding of the limiting late endosomal membrane to generate intraluminal vesicles (ILVs), mature within multivesicular bodies (MVBs). Subsequently, fusion of MVBs with plasma membrane results in the release of ILVs to the extracellular environment as exosomes (Han et al. 2022; Arya et al. 2024). Along with the biogenesis, a variety of membranal and cytoplastic cargos of proteins, nucleic acids, lipids and metabolites are sorted into either lipid bilayer or intraluminal space (Wan et al. 2019; Gurung et al. 2021). The transfer of these bioactive cargos between cells plays critical role in maintaining biological functions or promoting pathogenesis.

Compared to its normal origin cells (e.g., neural progenitor cells), GBM cells can substantially secrete exosomes, which are involved in promoting angiogenesis, immune escape, invasion and therapeutic resistance (Hu et al. 2022; Xia et al. 2023; Qin et al. 2025). Previous studies uncovered that tumour-derived exosomes may exacerbate chemoresistance by transferring specific miRNAs and proteins. For example, exosomal miR-1238 from TMZ-resistant GBM cells could be taken up by sensitive cells and promote resistance via downregulation of caveolin-1 (CAV1) and activation of EGFR/PI3K-Akt signalling (Ma et al. 2024). Moreover, exosome-transmitted lncRNA lnc-TALC could modulate the tumour microenvironment through microglia activation and complement secretion, enhancing DNA repair and reducing TMZ-induced cytotoxicity (Li et al. 2021). More recently, exosomal transfer of metabolic enzyme pyruvate kinase M2 (PKM2) has also been implicated in driving TMZ resistance under hypoxic conditions (Li et al. 2024). These findings underscore how exosomes act as driver of chemoresistance determinants-miRNAs, noncoding RNAs, and proteins-fundamentally altering DNA repair, survival signalling, metabolism and tumour microenvironment, thereby undermining TMZ efficacy. Although the role of exosomes in chemoresistance is increasingly recognised, their specific involvement in TMZ resistance in GBM remains largely unknown (Chen et al. 2021).

In this study, we aimed to investigate the relationship between exosomes and TMZ resistance in GBM cells after exposure to TMZ treatment. We found that GBM cells treatment with different chemotherapeutic agents, including TMZ, doxorubicin (DOX) and cisplatin (CDDP), induced enhanced exosome secretion compared to untreated cells. Despite an increased secretion, exosomes derived from TMZ-treated cells could still maintain typical morphology, size distribution and zeta potential, with only slight fluctuation in expression profile of surface markers, such as CD9, CD63 and CD81. Western blot analysis revealed that increased expression of p53 (a critical tumour-suppressing protein) might be the predominant reason to promote exosome secretion by upregulating six transmembrane epithelial antigen of prostate 3 (STEAP3) expression under stress condition. In vitro cellular uptake studies demonstrated that TMZ-induced exosomes were preferentially taken up by cognate tumour cells and brain endothelial cells, in contrast to non-induced exosomes. More importantly, we identified that pre-treatment with TMZ-induced exosomes could reduce the sensitivity of C6 cells to TMZ. We recognised that exosome secretion may serve as a potent TMZ resistance mechanism via enhancing anti-apoptotic ability of GBM cells towards TMZ exposure. Further proteomic analysis revealed an overall upregulation of protein profiles in TMZ-induced exosomes, with particular enrichment of proteins associated with PI3K/AKT pathway, of which the activation is considered significant cause of chemoresistance in cancer therapy. We thus speculated that the upregulated exosomal proteins may be a strategic mechanism by which cells tended to acquire resistance to TMZ. Collectively, our findings demonstrated that chemotherapeutic agents could profoundly promote exosome secretion and the TMZ-induced exosome secretion may serve as a potent resistance mechanism. These results not only provide a new insight of the role of exosomes in therapeutic resistance but also underscore the therapeutic potential of blocking exosome biogenesis to overcome TMZ resistance.

2 | Methods

2.1 | Cell Culture and Preparation

C6, bEnd.3, BV-2 and N2A cells were cultured in DMEM basic (1×) medium (Gibco, USA) containing 10% fetal bovine serum (FBS, PAN, Germany), 1% penicillin–streptomycin (Gibco, USA). DC2.4 cells were cultured in RPMI-1640 medium (Gibco, USA) containing 10% FBS and 1% penicillin–streptomycin. GL261 cells were cultured in DMEM medium containing 10% FBS, 1% penicillin–streptomycin, 1% glutamine (Gibco, USA) and 1% HEPES (Gibco, USA). Subcultures were maintained in humified incubator with 5% CO_2 supply at 37°C, and all experiments were performed during the logarithmic phase of cell growth.

2.2 | MTT Assay

To determine the half maximal inhibitory concentration (IC_{50}) of different kinds of drugs on C6 cells, the cell viability was tested. Cells were harvested, centrifuged and seeded into 96-well plates

at a density of about 1×10^4 cells per well, and then treated with TMZ and CDDP for 24 h incubation. 3-(4,5-Dimethylthiazol-2-yl)-2,5-diphenyltetrazoliumbromide (MTT, 5 mg/mL in PBS) was diluted 20 times with medium and added into 96-well plates with 100 μL per well. After incubating for 4 h, MTT solution in plates was discarded and 50 μL dimethyl sulfoxide (DMSO) was added in each well. The plates were placed in a constant temperature shaker at 37°C for 30 min with 75 rpm/min and the absorbance was measured at 570 nm with microplate reader (BioTek, USA).

2.3 | Chemotherapy Treatment and Exosome Purification

For the experimental group, cells were cultured in T25 flask for 24 h and then incubated with 100, 300 and 600 μg/mL TMZ for another 24 h, then the supernatant containing TMZ was discarded, the cells were rinsed with PBS, and 10 mL exosome-depleted DMEM was added to every T25 flask, the supernatant was collected after culturing at 37°C for 24 h. The number of cells in each T25 flask was calculated, respectively. In the control group, the supernatant was discarded after 24 h culture without treatment, 10 mL exosome-depleted DMEM was added, and the supernatant was collected after 24 h culture. Treatment of cells with DOX and CDDP was similar to TMZ treatment, with altered incubation dose of DOX at 1, 3, 6 and 9 μg/mL and of CDDP at 100, 200 and 300 μg/mL.

C6 cells-derived exosomes were isolated from the supernatant by a sequential ultracentrifugation process, as previously reported (Li et al. 2017). Briefly, cells were removed from the supernatant by centrifugation at 300 × *g* for 10 min followed by removing debris at 2000 × *g* for 30 min. Then the supernatants were centrifuged at 10,000 × *g* for 30 min to remove apoptotic bodies and large cell debris (Thermo Scientific, USA). In the end, the supernatants were transferred to ultracentrifuge tubes and then centrifuged at 100,000 × *g* for 70 min (Beckman ultracentrifuge, Beckman Coulter). The pellets were further washed and re-suspended in 10 mL PBS and ultracentrifuged for the second time with 100,000 × *g* for 70 min. Exosomes were finally resuspended in 300 μL PBS and stored in −80°C for the further study.

Likewise, bEnd.3, GL261, BV-2 and N2A cells were also treated with TMZ, DOX and CDDP at a certain concentration of 100 μg/mL, 300 μg/mL and 600 μg/mL, 1 μg/mL, 3 μg/mL, 6 μg/mL and 9 μg/mL and 100 μg/mL, 200 μg/mL and 300 μg/mL, respectively. Cells without any treatment were set as the control group. Cells after treatment were also calculated and the exosomes were collected from supernatant after ultracentrifuged.

2.4 | Exosome Characterisation

The size and particle number of isolated exosomes were analysed by nanoparticle tracking analysis (NTA) using the ZetaView instrument (Particle Metrix, Germany). Twenty microlitres of the resuspended exosomes were diluted in 2 mL PBS at the ratio of 1:100. The diluted sample was injected into the instrument by 5 mL injection syringe. Software settings for capture and analysis were listed as followed: min bright = 30, min size = 10, max size = 1000, sensitivity = 70, shutter = 100. The zeta potential of isolated exosomes was determined by dynamic laser scattering (DLS, Malvern Nano-s, England). The morphology of isolated exosomes was verified by transmission electron microscope (TEM, FEI, USA) imaging following the protocol. Exosomes samples were first diluted in PBS to a concentration of 10–50 μg/mL. Ten microlitres aliquot of the exosome suspension was applied onto a formvar/carbon-coated copper grid and allowed to adsorb for 5–10 min at room temperature. Excess liquid was gently removed with filter paper and a drop of Milli-Q water was used to wash away contaminants. The grid was negatively stained with 2% (w/v) uranyl acetate for 1–2 min. After carefully removing the excess stain, the grid was air-dried for 10–15 min at room temperature. The images were performed using a TEM operated at an accelerating voltage of 80–100 kV.

2.5 | BCA Assay

Protein concentrations of lysates were determined using a bicinchoninic acid (BCA) assay before western blot analysis. Cells were lysed in ice-cold cell lysis buffer supplemented with protease and phosphatase inhibitors. Lysates were incubated on ice for 30 min and centrifuged at 12,000 × *g* for 15 min at 4°C to remove cell debris. The supernatant was collected, and aliquots were stored at −80°C until use next time. A stock solution of bovine serum albumin (BSA) was diluted with PBS buffer to generate a series of standards ranging from 0 to 2000 μg/mL. Immediately before use, Reagent A and Reagent B were mixed at a 50:1 ratio to form the BCA working reagent, according to the manufacturer's instructions. For each standard and unknown sample, 12.5 μL of solution was added to a 96-well plate. Subsequently, 100 μL of the BCA working reagent was added to each well and gently mixed. The plate was incubated at 37°C for 30 min. Absorbance was measured at 562 nm using a microplate spectrophotometer. A standard curve was generated from the BSA dilutions, and protein concentrations of the experimental samples were calculated using linear regression. Each sample was assayed in triplicate, and results were averaged to minimise technical variability.

2.6 | Western Blot

Equal amounts of protein (30 μg) were mixed with 5×SDS loading buffer and denatured at 99°C for 10 min. Samples were separated by SDS-PAGE on 10% polyacrylamide gels and transferred onto nitrocellulose (NC) membrane (Millipore, USA) using a wet transfer system. Membranes were blocked with 5% skimmed milk in Tris-Buffered Saline with Tween-20 (TBST) for 2 h at the room temperature, followed by the incubation with primary antibodies overnight at 4°C. After washing three times with TBST, membranes were incubated with appropriate secondary antibodies for 1 h at room temperature. Protein bands were visualised using enhanced chemiluminescence (ECL) reagents (Jiangsu Cowin Biotech Co., Ltd, China) and imaged with a 5200 multiautomated chemiluminescence system (Tianneng, Shanghai, China).

2.7 | Nanoflow Cytometry Analysis

Purified exosome samples were first diluted in PBS to achieve a particle concentration within the optimal detection range

(1×10^8–1×10^9 particles/mL). For fluorescence labelling, exosomes were incubated with antibodies conjugated with a fluorescence. Samples were loaded into the nanoflow cytometer and data were collected using the instrument's standard settings for small particle detection. At least 100,000 events per sample were recorded. Side scatter (SSC) and fluorescence signals were used to determine particle size and the protein expression.

2.8 | NanoView Microarray for Characterisation of Exosomes Surface Markers

Supernatant of cell culture was collected and then centrifuged at $300 \times g$ for 10 min, $2000 \times g$ for 30 min and $10{,}000 \times g$ for 30 min to remove cell debris as much as possible. The experimental procedure and instrument were provided by Quantum Scientific Instruments Trading (Beijing) Co., Ltd with a ExoView Exosome Kit. The supernatant after centrifuging was collected and diluted with the exosomes binding buffer (Solution A, pH7.4) at 1:10 for exosomes derived from 100 and 300 μg/mL TMZ treated cells and 1:30 for exosomes derived from 600 μg/mL TMZ treated cells. Fifty microlitres of diluted sample was dropped on the microarray chips for incubation overnight. Each microarray chip was precoated with capture antibodies CD9 and CD81. The chips were washed four times with Solution A at 150 rpm/min for 3 min each time. After washing, 300 μL blocking solution containing three detection antibodies, including CF488-conjugated CD9 (clone MZ3, rat, Biotium), CF555-conjugated CD81 (clone Eat-2, rat, Biotium) and CF647-conjugated CD63 (clone NVG-2, rat, Biotium), was used to incubate with each chip for 1 h at room temperature under protection from light. Following, microarray chips were washed with Solution A, Solution B and distilled water sequentially. Finally, the chips were airdried for imaging by ExoView R200 (NanoView Biosciences, USA).

2.9 | Cellular Uptake

Cellular uptake of exosomes was evaluated using fluorescently labelled exosomes. Exosomes were first labelled with PKH26 dye (Solarbio, China) according to the manufacturer's instructions. In brief, isolated exosomes were resuspended in Dilute C, mixed with PKH26 dye solution and incubated for 5 min at room temperature with gently mixing. Excess dye was removed by ultracentrifugation at $100{,}000 \times g$ for 70 min at 4°C. The labelled exosomes pellet was resuspended in PBS at the desired concentration. Recipient cells were seeded in 24-well plates at a density of 5×10^4 cells per well and cultured overnight. Cells were then incubated with PKH26-labelled exosomes (1×10^9 particles per well) for 4, 8 and 24 h at 37°C in a humidified incubator with 5% CO_2. After incubation, cells were washed twice with PBS to remove uninternalised exosomes. Finally, cells were resuspended in 300 μL PBS for flow cytometry analysis (BD Bioscience, USA).

2.10 | Apoptosis

Cell apoptosis was detected using an Annexin V-FITC/propidium iodide (PI) apoptosis detection kit (Yeasen, China) according to the manufacturer's instructions. Briefly, cells were seeded in 12-well plates at a density of 6×10^4 per well. After 24 h of cultivation at 37°C, exosomes derived from 100, 300 and 600 μg/mL TMZ-treated C6 cells were added to the plates (7.5×10^9 particles per well). Cells without exosomes incubation served as negative control. After incubation for 24 h, TMZ was added at the concentration of 300 μg/mL. After incubation for 24 h, cells were harvested and then washed twice with cold PBS, and resuspended in 1×binding buffer at a concentration of 1×10^6 cells/mL. Subsequently, 5 μL of Annexin V-FITC and 10 μL of PI were added to 100 μL of the cell suspension. The mixture was gently vortexed and incubated for 15 min at room temperature in the dark. After adding 400 μL of binding buffer, samples were immediately analysed by flow cytometry (BD Bioscience, USA). Data were processed using FlowJo software and apoptotic cells were quantified as the sum of early apoptotic (Annexin V positive, PI negative) and late apoptotic (Annexin V positive, PI positive) populations. All experiments were performed in at least three independent biological replicates. The same experimental procedures applied to C6 cells were also performed in GL261 cells under identical conditions.

2.11 | Assessment of Chemotherapy Sensitivity Following Treatment With Exosomes From TMZ-Treated Tumour Cells

C6 cells were seeded in a 96-well plate at an appropriate density and cultured overnight. Then the cells were incubated with the exosomes, which were isolated from TMZ-treated C6 cells. After pre-treatment with exosomes isolated from TMZ-treated cells, C6 cells were further exposed to various concentrations of TMZ for 24 h. Cell viability and chemotherapeutic sensitivity were assessed using a MTT assay. Absorbance was measured at 570 nm using a microplate reader and cell viability was calculated relative to untreated cells. IC_{50} values were determined using nonlinear regression analysis.

2.12 | Preparation of Ultrathin Cell Sections

Cells were cultured under the specified experimental conditions and harvested at the desired time point. After washing twice with PBS, cells were fixed with 2.5% glutaraldehyde in 0.1 M cacodylate buffer (pH 7.4) for 2 h at 4°C. Following primary fixation, cells were washed three times with 0.1 M cacodylate buffer and post-fixed in 1% osmium tetroxide (OsO_4) for 1 h at room temperature. Samples were then dehydrated through a graded ethanol series (30%, 50%, 70%, 90% and 100%, 10 min each) and infiltrated with epoxy resin overnight. Resin-embedded samples were polymerised at 60°C for 48 h. Ultrathin sections (70 nm) were cut using an ultramicrotome equipped with a diamond knife. Sections were collected on copper grids and stained with 2% uranyl acetate for 10 min, followed by lead citrate for 5 min. After rinsing with distilled water and air drying, samples were examined under a transmission electron microscope at an accelerating voltage of 80–100 kV. Representative images were captured to assess cellular ultrastructure.

2.13 | Proteomic

Exosomes were isolated from conditioned medium of C6 cells with an ultracentrifugation protocol. All procedures were per-

formed at 4°C to preserve exosome integrity. To extract proteins, exosomes were lysed in radioimmunoprecipitation assay (RIPA) buffer supplemented with protease inhibitors (1:100, v/v) and sonicated on ice with 10 s for three times. Then the lysate was centrifuged at 12,000 × *g* for 10 min at 4°C to remove insoluble debris. The supernatant was collected as the protein extract and the total protein was quantified by a BCA assay with BSA standards. Protein samples were normalised to 50–100 μg for per analysis. For label-free quantitative proteomics, proteins were digested in solution to generate peptides. The peptides separation and mass spectrometry (MS) analysis were performed on a nano-LC system coupled to a mass spectrometer. Functional annotation was performed using DAVID for Gene Ontology (GO) and Kyoto Encyclopedia of Genes and Genomes (KEGG) pathway enrichment.

2.14 | Statistical Analyses

Multiple comparisons between different groups were analysed by one-way AVONA. A comparison between the experimental group and control group was analysed by the paired Student's *t* test. Significant differences are labelled ⋆ for $p < 0.05$, ⋆⋆ for $p < 0.01$ and ⋆⋆⋆ for $p < 0.001$.

3 | Results

3.1 | Chemotherapy Promotes Cellular Production of Exosomes

To understand the relationship between exosome secretion and chemotherapy resistance, the influence of TMZ on exosome secretion was first explored since TMZ is the first-line chemotherapeutic agent for GBM. To determine the appropriate incubation dose, MTT assay was performed and an incubation dose of 300 μg/mL close to IC_{50} was chosen for further investigation (Figure S1). At different incubation times, the total number of secreted exosomes showed no significant changes between TMZ-treated and untreated cells (Figure 1a). Surprisingly, TMZ-treated cells exhibited higher number of secreted exosomes after normalising to each cell compared with untreated cells, which was owing to inhibited cell proliferation resulted from TMZ treatment (Figure 1b). Increasing the incubation time led to a higher number of exosomes per cell, suggesting a correlation of incubation time. Despite increased secretion, TMZ-induced exosomes still maintained a similar size distribution and zeta potential to naturally secreted exosomes (Figure 1c, d). Moreover, transmission electron microscopy (TEM) images of TMZ-induced exosomes demonstrated a typical cup-shaped morphology (Figure 1g), validating that TMZ treatment had negligible influence on the physiochemical properties of exosomes. To further investigate the influence of TMZ dose on exosome secretion, gradient doses of 100, 300 and 600 μg/mL were applied. The results showed that treatment with TMZ at a dose of 600 μg/mL led to a marked increase in exosome secretion, which was probably attributed to increased apoptotic stress induced by TMZ (Figure 1e). Western blot was also performed to further validate successful exosome isolation. The exosomes were positive for CD63 and tumour susceptibility gene 101 (TSG101), while the negative marker calnexin was not detected, indicating minimal contamination. The results confirmed the purity and identity of the isolated exosomes and supported the reliability of subsequent functional analysis (Figure S2). Additionally, the impact of TMZ was further assessed in other types of cells to verify whether the TMZ-induced exosome secretion was cell type specific. Consistent with the observation in C6 cells, bEnd.3 (a murine brain capillary endothelial cell line), BV-2 (a murine microglia cell line), N2A (a murine neuroblastoma cell line) and GL261 (a murine glioma cell line) cells treated with TMZ also demonstrated an enhanced exosome secretion, confirming the nonspecific cytotoxicity of TMZ that can induce apoptotic stress towards both cancer cells and normal cells (Figure 1f).

Moreover, whether chemotherapeutic agents with different mechanisms can induce exosome secretion in both cancer cells and normal cells remain unknown. Therefore, two widely used chemotherapeutic agents were selected: DOX and CDDP. CDDP functions as a DNA crosslinking and apoptosis-inducing agent, which is often in combination with TMZ, Vincristine and Lomustine for clinical treatment of GBM. Based on MTT assay results, an incubation dose of 200 μg/mL close to IC_{50} was chosen for investigation (Figure S3a). In line with TMZ treatment, treatment with CDDP also significantly increased the number of exosomes per cell compared to untreated groups, with negligible influence on size distribution and zeta potential (Figure 1 h, Figure S3b, c). In addition, increasing the incubation dose of CDDP led to higher level of exosome secretion, revealing a correlation of incubation dose (Figure 1i). Similar trends were also observed across multiple cell types, indicating that CDDP was also able to promote the exosome secretion regardless of cell types (Figure 1j).

DOX, an anthracycline antibiotic with broad-spectrum antitumour effects, functions by damaging cancer cell through intercalating DNA base pairs and inhibiting the enzyme topoisomerase II. Accumulating studies proved that DOX can be effective treatment for GBM, although it faces challenges in reaching tumour site due to BBB. As expected, DOX treatment led to an increased number of exosomes per cell compared to untreated groups, particularly at 48 h post-treatment, which was consistent with TMZ and CDDP treatment (Figure 1k, Figure S4). An interesting finding was that DOX treatment at an incubation dose of 3 μg/mL DOX resulted in highest exosome secretion compared to 1, 6 and 9 μg/mL (Figure 1l). Overall, a dose-dependent behaviour of DOX-induced exosome secretion can be speculated. Furthermore, DOX treatment also promoted exosome secretion across cell types, confirming this finding that chemotherapy significantly induced exosome secretion in both cancer cells and normal cells (Figure 1m).

3.2 | Marker Expression of TMZ-Induced Exosomes

To explore the potent impact of TMZ treatment on surface markers expression profile, nano flow cytometry designed for quantitative analysis of nanoparticles at the single particle level was applied. The quantitative analysis showed that the expression of CD81 remained largely unchanged in TMZ-induced exosomes compared to untreated exosomes regardless of the concentration, while the expression of CD9 and CD63 was increased in positive correlation with concentration (Figure 2a, b). These results

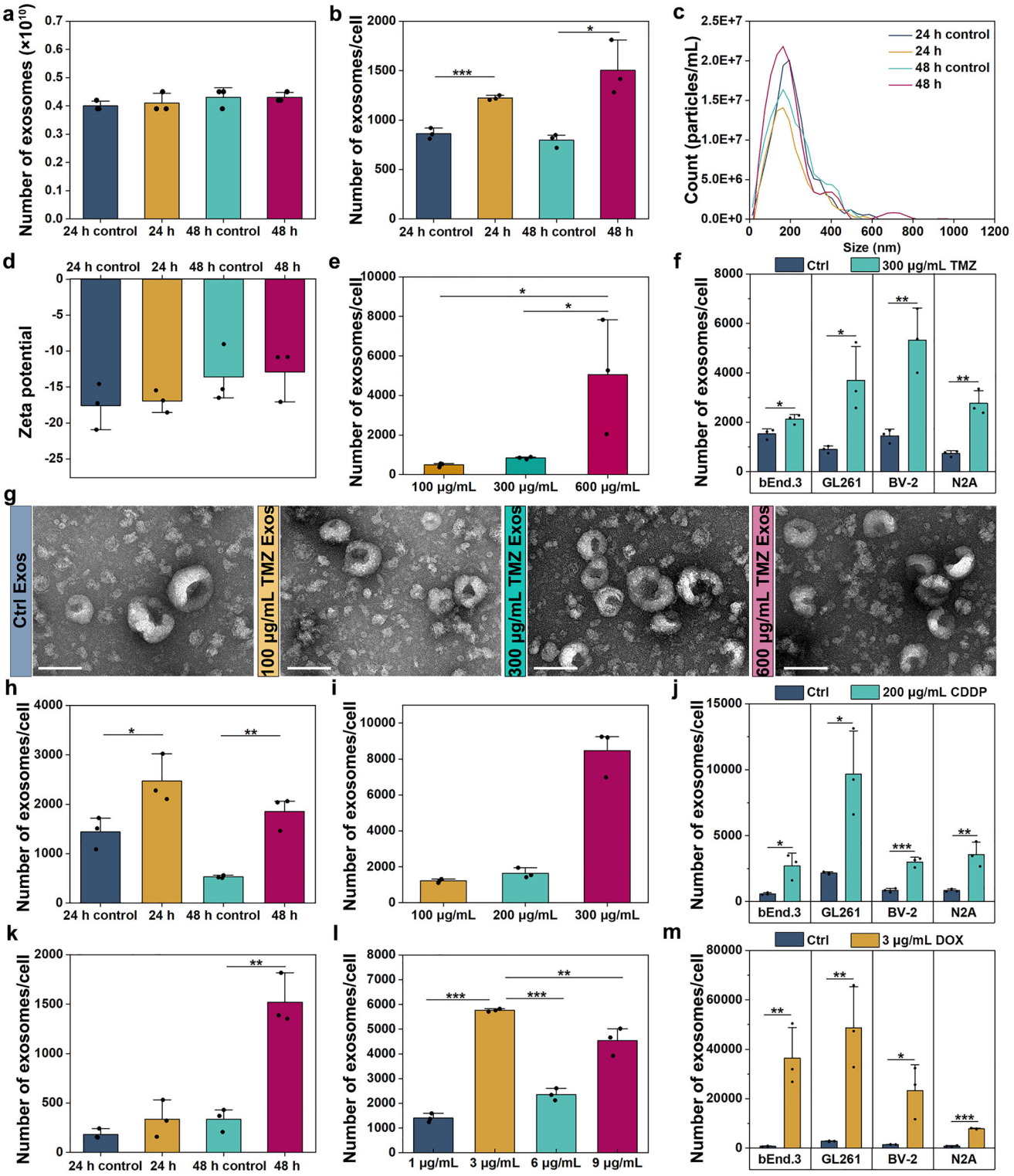

FIGURE 1 | Characterisation of chemotherapeutic agents-induced cellular production of exosomes. (a) The total particle counts of exosomes with and without TMZ treatment ($n = 3$). (b) Average cellular secretion rate for exosome production from both TMZ treated and untreated C6 cells ($n = 3$, each plot represents an independent experiment). (c) NTA analysis of size distribution of TMZ-induced exosomes, indicating the consistent size range compared to the control group exosomes without TMZ treatment. (d) Zeta potential profiles from TMZ-induced exosomes which is consistent with their control group without TMZ treatment ($n = 3$). (e) Average cellular secretion rate for exosomes after treatment with different concentration of TMZ ($n = 3$). (f) Average cellular secretion rate for exosomes in different cell types after exposure to TMZ ($n = 3$). (g) TEM images showing the morphology of TMZ-induced exosomes from C6 cells, which is consistent with the control group of native exosomes. Scale bar = 100 nm. Average cellular secretion rate for exosome production after treatment with CDDP (h) and DOX (k) ($n = 3$). Average cellular secretion rate for exosomes after treatment with different concentration of CDDP (i) and DOX (l) ($n = 3$). Average cellular secretion rate for exosomes in different cell types after exposure to CDDP (j) and DOX (m) ($n = 3$). Data are represented as mean ± SD ($n = 3$). *n* refers to independent biological experiments. ⋆$p < 0.05$, ⋆⋆$p < 0.01$ and ⋆⋆⋆$p < 0.001$. TMZ, temozolomide; CDDP, cisplatin; DOX, doxorubicin; NTA, nanoparticle tracking analysis.

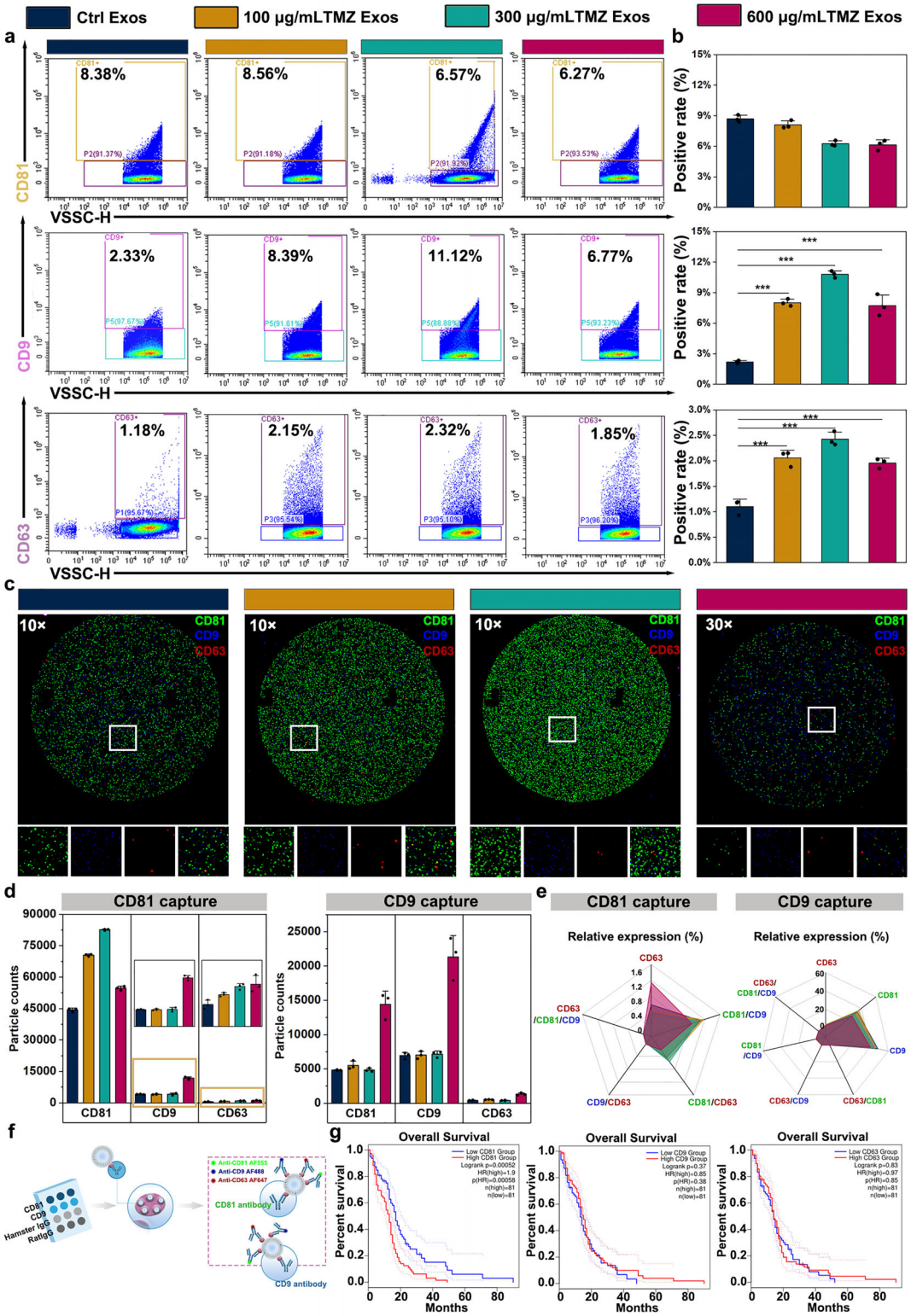

FIGURE 2 | Evaluation of the surface markers expression from TMZ-induced exosomes at the single particle level. (a) Representative nano flow cytometry plots of exosomes from different treatment ($n = 3$). (b) The quantification of the positive rate of CD81, CD9 and CD63 on exosomes surface ($n = 3$). (c) Representative fluorescent microarray imaging of $CD81^+$ (green), $CD9^+$ (blue) and $CD63^+$ (red) exosomes on CD81 capture spots. Bottom image frames are enlarged views of captured exosomes under each fluorescent channel as well as the overlay. (d) Particle counts of captured $CD81^+$, $CD9^+$ and $CD63^+$ exosomes from different exosomes sample conditions on CD81 and CD9 capture spots ($n = 3$). (e) Radar chart analysis of the relative co-expression level of multi-markers in various combinations from different exosomes sample conditions on both CD81 and CD9 capture spots. (f) Schematic diagram of sensitive multi-marker detection from exosomes captured on microarray chip spot. (g) GEPIA analysis of the correlation between CD81, CD9 and CD63 expression and patient overall survival. Data are represented as mean ± SD. n refers to independent biological experiments. ⋆⋆⋆$p < 0.001$. GEPIA, gene expression profiling interactive analysis; TMZ, temozolomide.

indicated that TMZ treatment may influence the certain surface markers expression of exosomes, whereas more investigations are required to uncover the underlying alteration in functionalities.

Meanwhile, a single-exosome microarray imaging technology from NanoView was employed to directly visualise and determine the surface markers expression. The capture antibody coated onto each microarray chip spot allows the capture-based immobilisation of exosomes from samples for further immune-probing with up to three fluorescently labelled antibodies (Figure 2f). Fluorescent images of CD81 capture spots clearly displayed each single exosome with either individual or colocalised probing antibodies (CD63 in red, CD81 in green and CD9 in blue) (Figure 2c). In comparison, fluorescent images of the isotype spots (HIgG or RIgG) exhibited much lower captured exosomes in same dilution rate, denoting the high affinity and specificity of CD81 and CD9 capture antibodies. In line with NTA results, total exosome counts captured in either CD81 spot or CD9 spot further confirmed the trend that TMZ treatment promoted exosome secretion and increasing TMZ concentration led to higher exosome secretion (Figure S5). In both CD81 and CD9 capture spot, the total counts of $CD81^+$ and $CD9^+$ exosomes were much higher than counts of $CD63^+$ exosomes, which was also consistent with the nano flow cytometry results. This finding was probably due to the nature of C6 cells-derived exosomes that were enriched in CD81 and CD9 expression, while poor in CD63 expression. Compared to untreated group, the total counts of $CD81^+$, $CD9^+$ and $CD63^+$ exosomes from TMZ-treated groups were all increased (Figure 2d). Furthermore, the relative percentage of three markers normalised to total counts also demonstrated an increased percentage of CD81, CD9 and CD63 expression on TMZ-induced exosomes, with particularly higher percentage of CD81 expression (Figure 2e). Collectively, TMZ treatment could induce upregulated expression of tetraspanins, whereas more investigation was required to confirm this finding since the results from nano-flow cytometry and microarray imaging were not entirely consistent. These differences may be attributed to methodological variations between the two platforms, including detection principles, assay sensitivity and sample types. For detection principles, nano-flow cytometer relies on fluorescence-based detection of individual exosomes in suspension, whereas NanoView captures exosomes based on immunoaffinity with antibody coated on chips. In terms of assay sensitivity, the two platforms exhibit distinct sensitivity and dynamic range due to their different detection modes. A nano-flow cytometer allows high-throughput analysis but may be less sensitive for low-abundance markers or weakly labelled exosomes. NanoView achieves higher sensitivity for specific markers by enriching exosomes through surface antibody capture, particularly those with strong antibody affinity. In addition, the analysed samples are also not identical: nano-flow cytometer is typically performed on isolated exosomes following purification, whereas NanoView directly analyse exosomes from cell culture supernatants without prior isolation. Overall, these methodological differences collectively may contribute to the observed discrepancies between the two platforms and should be carefully considered when interpreting and comparing exosome profiling results.

It has been revealed that CD81 is a canonical structural protein on the surface of exosomes that not only contributes to exosome biogenesis but also function as molecular guides for sorting of tetraspanin-enriched microdomain-associated proteins into exosomes (Lee et al. 2024). Therefore, the high expression of CD81 on TMZ-induced exosomes was more likely to be linked with enhanced exosome secretion capacity as well as specific functionalities. Additionally, the survival curves from gene expression profiling interactive analysis (GEPIA) database were analysed and the results showed that GBM patients with high CD81 expression exhibited shorter overall survival compared with those with low CD81 expression, suggesting that elevated CD81 expression on TMZ-induced exosomes may negatively impact patient prognosis. In contrast, CD9 and CD63 expression showed less correlation with GBM patient survival (Figure 2 g, Figure S6).

3.3 | p53-STEAP3-Dependent Exosome Secretion Pathway

Understanding the underlying mechanism involved in promoting exosome secretion after TMZ treatment is particularly important. As above mentioned, TMZ induces DNA damage primarily through the formation of DNA-methyl adducts, which can lead to DNA double-strand breaks (DSBs). These DSBs further activate the p53 protein, a major tumour suppressor protein that acts as a transcription factor to induce apoptosis or programmed cell death (Naumann et al. 2009). Six-transmembrane epithelial antigen of prostate 3 (STEAP3), also known as tumour suppressor-activated pathway 6 (TSAP6), contains a functional p53-binding site in its promoter and has been reported as a direct transcriptional target of p53 (Wang et al. 2021). The activation of p53 leads to increased STEAP3 expression, which in turn promotes p53-mediated apoptosis. Moreover, accumulating studies revealed that STEAP3 is a key regulator of exosome secretion and is partly dependent on p53 (Lespagnol et al. 2008). To determine the role of p53-dependent secretory machinery in TMZ-induced exosome secretion, western blot analysis of key proteins was performed. As expected, the results showed an increased p53 expression in C6 cells post-treatment with TMZ, particularly at a concentration of 300 and 600 μg/mL. Consistently, an increased expression of STEAP3 was observed as the concentration increased. Meanwhile, a decreased expression of B cell lymphoma-2 (BCL-2), a major anti-apoptotic protein, was also observed (Figure 3a, b). These results collectively suggested a correlation between TMZ-induced p53-STEAP3 upregulation and this machinery may play a dominant role in promoting exosome secretion, although direct causality remained to be formally established.

Given that STEAP3 plays a critical role in the formation of MVBs and the sorting of ILVs into the MVB lumen for eventual release as exosomes, we set out to directly observe the formation of MVBs and ILVs using bio-TEM. Images of untreated C6 cells clearly displayed the existence of MVBs, whereas very limited ILVs were found within MVBs lumen. As a sharp contrast, TMZ treatment not only significantly increased the number of MVBs but also increased the number of ILVs, which is consistent with enhanced exosome biogenesis. These observations supported the possibility that TMZ-induced exosome secretion might be linked to the activation of p53-dependent secretory machinery, of which STEAP3 may act as a critical factor in MVB and ILV formation (Figure 3c–e). These results suggested a proposed mechanism that TMZ exposure was associated with the activation of p53-STEAP3 signalling pathway, accompanied by increased

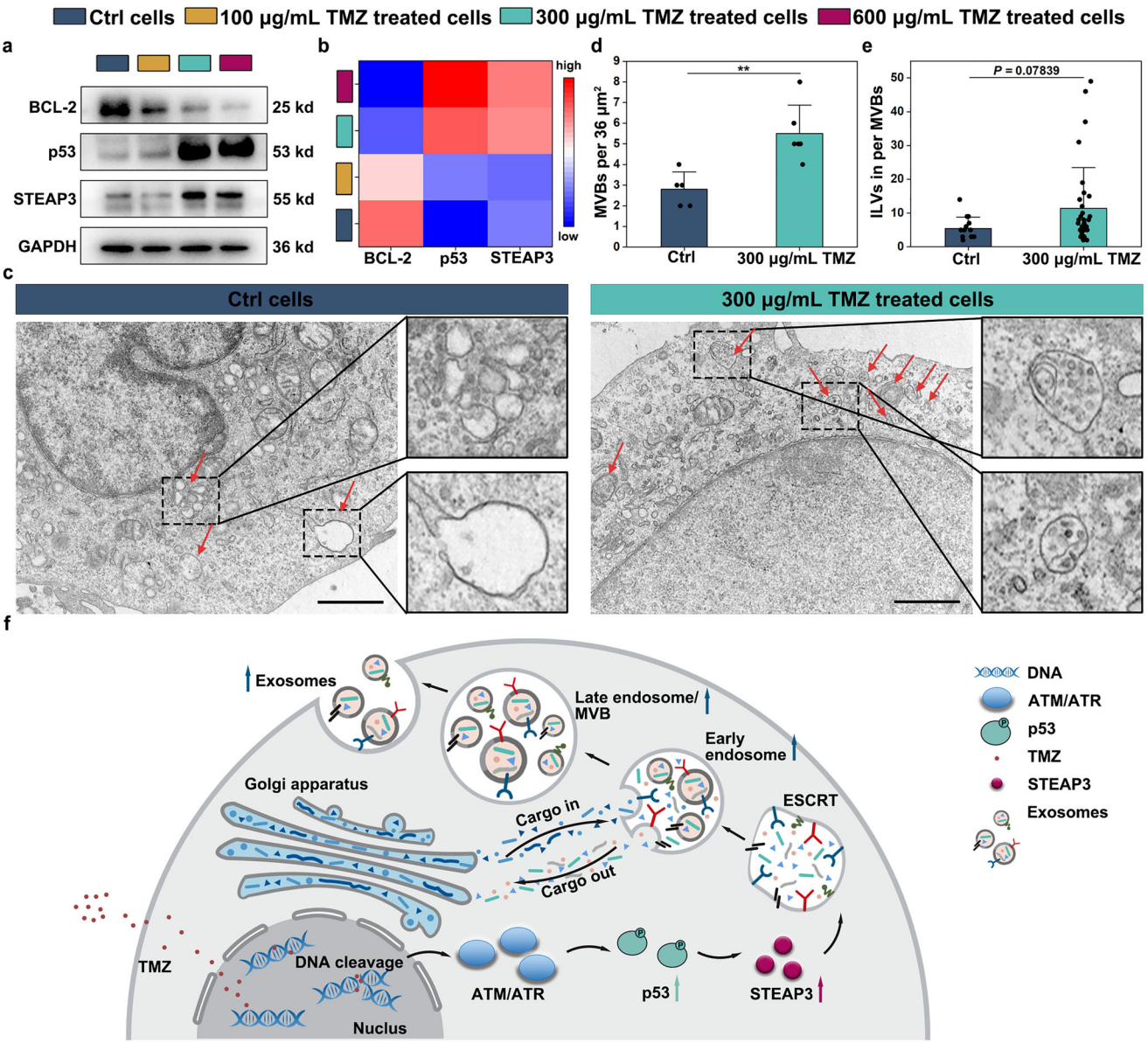

FIGURE 3 | p53-STEAP3-dependent pathway is associated with increased exosome secretion under TMZ treatment. (a) Western blot analysis of BCL-2, p53 and STEAP3 in TMZ-treated C6 cells and control cells. (b) Relative protein expression heatmap. (c) Representative bio-TEM images of C6 cells treated with 300 μg/mL TMZ and control cells. Scale bar = 1 μm. (d) The number of MVBs per 36 μm^2 ($n = 5$). (e) The number of ILVs per MVB. (f) Schematic of a proposed mechanism for TMZ-induced exosome biogenesis. Data are represented as mean ± SD. n refers to independent biological experiments. $\star\star p < 0.01$. BCL-2, B cell lymphoma-2; ILV, intraluminal vesicle; MVB, multivesicular body; STEAP3, six-transmembrane epithelial antigen of prostate 3; TEM, transmission electron microscope; TMZ, temozolomide.

exosome biogenesis with the increased numbers of MVBs and ILVs (Figure 3f), although further functional studies are required to establish a causal relationship.

3.4 | In Vitro Evaluation of Cellular Uptake

The internalisation of exosomes by recipient cells contributes to the basis of intercellular communication. Thus, cellular uptake of TMZ-induced exosomes by different types of cells was evaluated to determine whether TMZ treatment influence the uptake behaviour. Flow cytometry analysis displayed that the uptake of PKH26-labelled exosomes by different cells increased over time, presenting a time-dependent manner. In C6 and bEnd.3 cells, the uptake of TMZ-induced exosomes was higher than that of non-induced exosomes at each time point, with the highest uptake of exosomes derived from cells treated with 300 μg/mL TMZ, suggesting that these TMZ-induced exosomes are more preferentially to be internalised. This finding was probably attributed to the up-regulated expression of tetraspanins, which can promote TMZ-induced exosome uptake by recipient cells by directly binding to receptors or indirectly organising microdomains that enriched with integrins (Jankovičová et al. 2020; Das et al. 2024). In BV-2 cells, however, the results showed an opposite trend that the uptake of TMZ-induced exosomes was slightly decreased compared to non-induced exosomes. It

could be speculated that microglia recognise and phagocytose foreign substance through multiple receptors, such as triggering receptor expressed on myeloid cells 2 (Trem2), complement receptor-3 (CR3) and scavenger receptors (SRs) (Fu et al. 2014). However, evidences uncover that tetraspanins may compromise their functions by interacting with these receptors and associated signalling molecules to affect activity and phagocytosis (Brosseau et al. 2018). Surprisingly, the uptake of TMZ-induced exosomes by DC2.4 cells was close to untreated exosomes at each time point, presenting a different trend to neither C6 and bEnd.3 cells nor BV-2 cells. Despite an overlap in phagocytosis-related receptors between microglia and DCs, such as CR3 and SRs, DCs as the professional antigen-presenting cells may involve specific internalisation mechanisms that are not affected by tetraspanins (Figure 4a, b). Overall, the TMZ-induced exosomes were able to be internalised by cells, while the internalisation behaviours depended on cell types.

3.5 | Exosome-Mediated TMZ Resistance Post-Treatment

TMZ resistance is the major reason contributing to modest survival benefit, and multiple intrinsic and acquired mechanisms are well-documented to be involved in the TMZ resistance. However, whether TMZ-induced exosomes contributed to the TMZ resistance remains unknow. Considering that enhanced exosome secretion and subsequent uptake by surrounding cells within GBM lesion occurred following TMZ treatment, we hypothesised that exosome secretion and cellular uptake may exacerbate the TMZ resistance. To confirm this hypothesis, we first performed Annexin V-FITC/PI staining to evaluate the impact of TMZ-induced exosomes on the TMZ sensitivity of C6 cells. The results showed that pre-incubation with TMZ-induced exosomes isolated from different conditions led to notably reduced late apoptosis of C6 cells post-exposure to free TMZ again compared to non-induced exosomes, indicating that TMZ-induced exosomes may reduce the TMZ sensitivity of cells (Figure 4c, d). The apoptosis experiment was also performed in GL261 cells to evaluate that the observed effect is not C6-specific. In line with the findings in C6 cells, flow cytometry analysis of GL261 cells also exhibited a similar trend that pre-treatment with TMZ-induced exosomes led to reduced apoptosis, particularly under 300 μg/mL TMZ concentration, reflecting increased TMZ resistance (Figure S7). These findings collectively suggested that the exosome-mediated TMZ resistance may be a broad phenomenon, rather than being restricted to a single cell line. Next, the MTT assay was used to detect the effect of TMZ-induced exosomes on cell viability of C6 cells. Consistently, the results showed that pre-incubation with TMZ-induced exosomes led to increased cell viabilities post-exposure to free TMZ, with an increased IC_{50} compared to non-induced exosomes group (Figure 4e, f). However, as the full workflow was not systematically replicated in GL261 cells, these results should be considered as supportive rather than definitive evidence, and the generalisability of this effect across GBM models requires further investigation. Collectively, both apoptosis and cell viability studies supported our hypothesis that TMZ-induced exosomes may promote TMZ resistance of GBM cells. This phenomenon was probably owing to that TMZ-induced exosomes may carry STEAP3, which not only promote apoptosis but also contribute to survival.

3.6 | Proteomics Analysis of Exosomal Proteins

Mounting evidences revealed that exosomal miRNA, such as miR-1238 and miR-21, plays a crucial role in promoting the chemoresistance of GBM, indicating that exosomal cargoes may drive TMZ resistance (Yin et al. 2019; Cheng et al. 2022). Exosomal proteins serve as essential mediators of cellular function and play central roles in cancer progression and tumourigenesis. However, whether exosomal proteins also contribute to TMZ resistance remains largely unknown. Thus, we further investigated the protein profiles of TMZ-induced exosomes as well as potential alterations by proteomic analysis. To visualise the multivariate data and reveal potential patterns for further investigation, a principal component analysis (PCA) was performed (Figure 5a). The PCA plot indicated that the first principal component (PC1) accounted for 46.63% of the total variance, while the second principal component (PC2) explained an additional 11.38%. For TMZ-induced exosomes group at the concentration of 300 and 600 μg/mL, the dispersed distribution of data plots indicated substantial within-group variability, which may attribute to intrinsic biological heterogeneity among samples. In contrast, the plots within other groups were more tightly clustered, reflecting a more uniform distribution of quantitative proteomic profiles. Comparing to the control group, the plots in TMZ-induced exosomes group were clearly separated, indicating a clear difference in overall characteristics. Furthermore, the Pearson correlation plot was applied to demonstrate the degree of correlation among the four groups. Most correlation coefficients between control exosomes and TMZ-induced exosomes were less than 0.5, indicating the pronounced differences between the two groups at the protein level (Figure 5b). To pinpoint specific differentially abundant proteins (DAPs) that might play key roles in TMZ resistance, we next conducted differential abundance analysis. In contrast with control exosomes, hierarchical clustering analysis showed that some of the proteins were upregulated in TMZ-induced exosomes (Figure 5c). Taken together, these results from PCA, Pearson correlation and hierarchical clustering analysis indicated alterations in protein profiles in TMZ-induced exosomes compared with control group.

Comparing the magnitude of protein abundance changes ($\log_2$fold change) with the statistical significance of the difference (adjusted p value). A threshold of adjusted p value < 0.05 and $|\log_2 FC| > 1.5$ were applied for filtering. Consistent with hierarchical clustering analysis, all DAPs expression in the TMZ-induced exosomes groups were upregulated compared to non-induced exosomes group (Figure 5d). These DAPs are involved in multiple biological functions that may collectively be associated with tumour cell tolerance and resistance to chemotherapy rather than acting as independent resistance factors (Figure 5e). Chaperones and stress-response proteins, such as HSP90AB1 (Babi et al. 2022) and HSPA5 (Xu et al. 2025), support proteostasis and cell survival under TMZ-induced stress. Proteins associated with cytoskeletal remodelling, extracellular matrix interactions and epithelial-mesenchymal transition, such as CFL1 (Wang et al. 2013), ANXA2 (Wang et al. 2019), FN1 (Song et al. 2021) and CSPG4 (Xiong et al. 2025), are linked to enhanced invasiveness and aggressive phenotypes that are frequently coupled with chemoresistance. Metabolic regulators, such as ALDOA (Deng et al. 2025), a critical glycolytic enzyme that

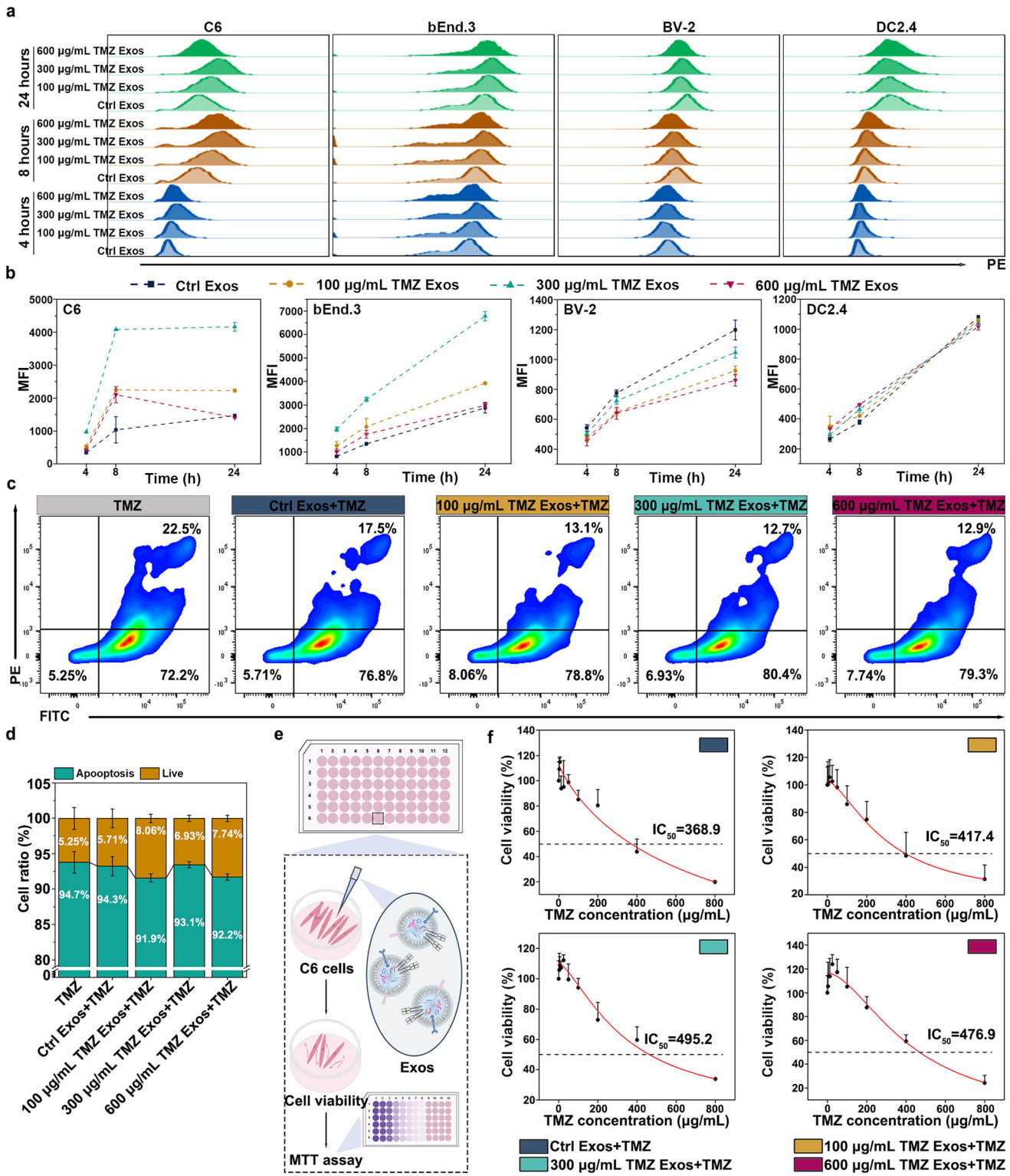

FIGURE 4 | In vitro evaluation of cellular uptake and exosome-mediated chemoresistance of temozolomide (TMZ)-induced exosomes. (a) Representative flow cytometry histogram of cellular uptake of TMZ-induced exosomes and control exosomes by C6, bEnd.3, BV-2 and DC2.4 cells at 4, 8 and 24 h. (b) Mean fluorescence intensity (MFI) quantification of (a) ($n = 3$). (c) Representative flow cytometry plots of apoptosis in C6 cells following incubation with control or TMZ-induced exosomes and then exposure to TMZ at a concentration of 300 μg/mL. (d) The quantification of the apoptotic and live cells ($n = 3$). (e) Experimental schematic of the impact of TMZ-induced exosomes on C6 cell viability. (f) Cell viability of C6 cells following incubation with control or TMZ-induced exosomes and exposure to TMZ at a concentration of 300 μg/mL ($n = 6$). Data are represented as mean ± SD. *n* refers to independent biological experiments.

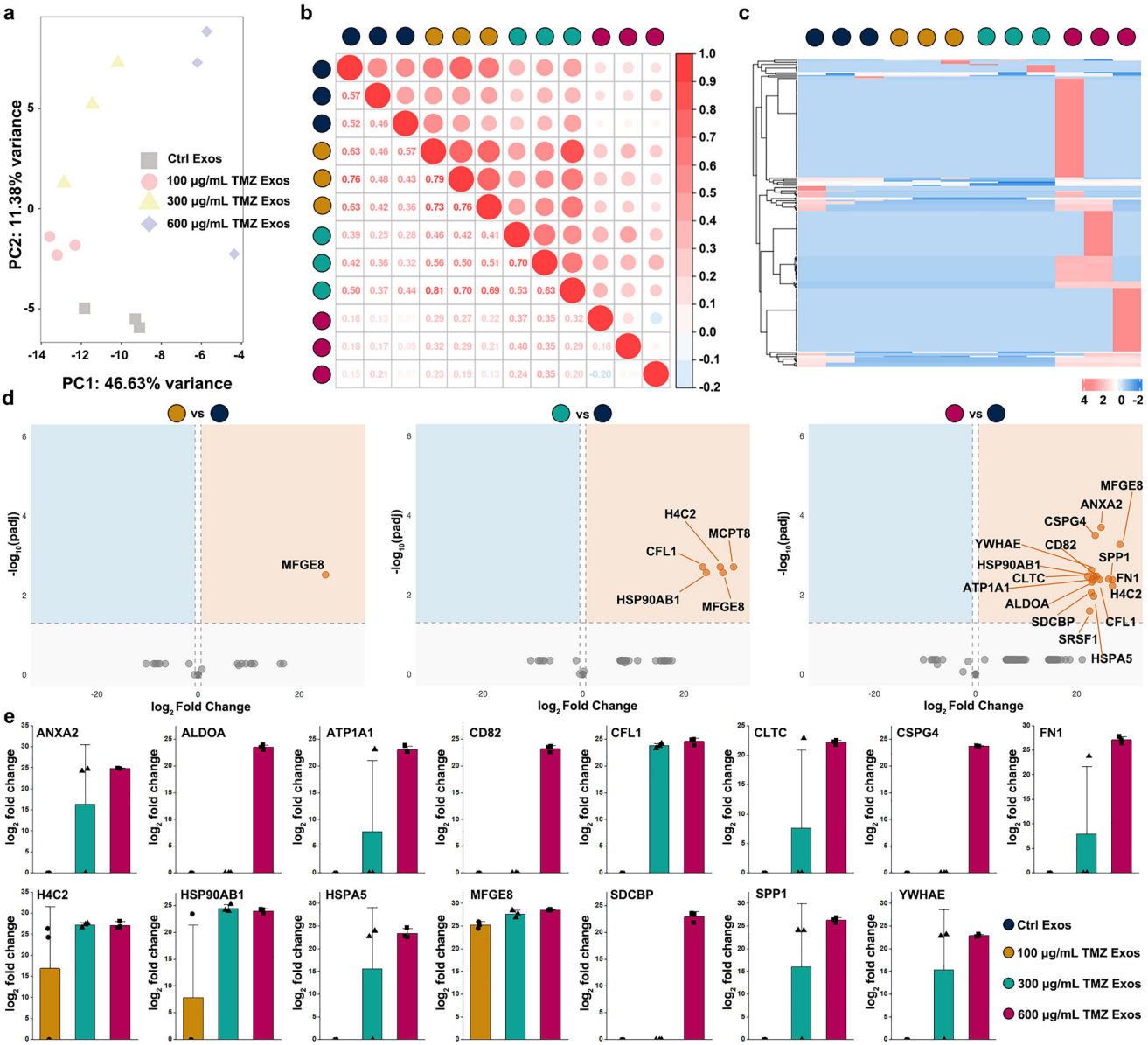

FIGURE 5 | Proteomic analysis of control and TMZ-induced exosomes. (a) PCA plot illustrates the variance in the full proteomics profiles between different groups ($n = 3$). The first two principal components, PC1 and PC2, represent 46.63% and 11.38% of the total variance. (b) Pearson correlation coefficient matrix plot of multiple groups ($n = 3$). The correlation coefficient was represented by a colour scheme from blue (negative correlation) to red (positive correlation). (c) Hierarchical clustering heatmap shows the expression pattern of DAPs in exosomes. The colours from blue to red indicate the increasing levels of proteins. (d) Volcano plots of TMZ-induced versus control exosomes proteomes at TMZ concentration of 100 μg/mL (left), 300 μg/mL (middle) and 600 μg/mL (right). Orange: upregulation, blue: downregulation. (e) The DAPs in exosomes isolated from different conditions ($n = 3$). Data are represented as mean ± SD. *n* refers to independent biological experiments. DAP, differentially abundant protein; PC1, first principal component; PC2, second principal component; PCA, principal component analysis; TMZ, temozolomide.

drives metabolic reprogramming and has been linked to therapy resistance, and ATP1A1 (Soumoy et al. 2024), which participates in survival signalling pathways, collectively facilitate tumour adaptation under therapeutic pressure. Vesicle trafficking and exosome biogenesis-related proteins, such as CLTC (Xie et al. 2022) and SDCBP (Ghossoub et al. 2014), may contribute to the selective sorting and dissemination of resistance-associated cargo. Epigenetic and transcriptional regulators, including H4C2 (Simon et al. 2020) and SRSF1 (Nehrbas et al. 2020), may further modulate chromatin organisation and stress-responsive gene expression programs that support adaptive tumour cell states. Other proteins, including MFGE8 (Wu et al. 2020), YWHAE (Fan et al. 2023) and SPP1 (Eun et al. 2023), participate in pro-survival and anti-apoptotic signalling pathways, thereby potentially contributing to resistance to chemotherapy. It was worth noting that the expression of metastasis suppressor CD82, a tetraspanin protein involved in cell adhesion, migration, signalling and membrane organisation, was also upregulated. However, its specific role in exosomes under chemotherapeutic stress requires further investigation. To further validate the

proteomic findings, enzyme-linked immunosorbent assay (ELISA) was performed to determine the levels of a subset of representative DAPs (e.g., HSP90AB1 and FN1) in different groups of exosomes. The results demonstrated that the levels of FN1 and HSP90AB1 proteins in TMZ-induced exosomes were much higher than that in non-induced exosomes, with up to two- and six-fold increase, respectively, which was consistent with the proteomic data (Figure S9). Collectively, all these results confirmed the reliability of the omics analysis as well as the finding that TMZ treatment may induce upregulated protein expression in exosomes. Together, we attributed the upregulated proteins to TMZ-induced cellular stress that caused tumour cells to alter intracellular process, leading to the enrichment of proteostasis, cell survival, phenotypic switching, metabolic adaptation and biogenesis-associated proteins in exosomes. The upregulation of proteins profile may reflect a self-protecting and strategic mechanism by which tumour cells tended to maintain homeostasis, promote survival, switch phenotype to become more adaptable to TMZ treatment, eventually leading to TMZ resistance. Moreover, the TMZ-induced exosomes with upregulated DAPs may further promote homeostasis, cell survival, metabolic adaptation of adjacent tumour cells following internalisation, therefore enhanced the TMZ resistance of adjacent cells, which also well explained the reduced TMZ sensitivity of C6 cells after pretreatment with TMZ-induced exosomes.

To further investigate the biological functions associated with the identified protein profiles, GO enrichment analysis was performed. The analysis showed that upregulated DAPs were significantly enriched in specific biological process, cellular component and molecular function (Figure 6a). In terms of biological process, the identified DAPs were predominantly related to regulation of cell size, growth and morphology, as well as cellular responses to extracellular stress signals elicited by TMZ treatment. These processes are closely linked to membrane remodelling and adhesion-related pathways, which are commonly dependent on cytoskeletal dynamics and integrin-based interactions and are known to play essential roles in endosomal trafficking and exosome biogenesis under chemotherapeutic stress. At the subcellular level, the upregulated DAPs were strongly associated with membrane-bounded compartments, particularly EVs and exosomes, along with secretory granule- and plasma membrane-related domains. These enriched cellular components were consistent with increased vesicle-associated membrane compartments and trafficking processes that underlied exosome biogenesis and secretion following TMZ exposure. Functionally, the proteome of TMZ-induced exosomes exhibited significant enrichment in phospholipid-binding activities, including phosphatidylserine-and phosphatidylinositol-related lipid binding, as well as binding to integrins, cell adhesion molecules, heat shock proteins, ubiquitin ligases and proteases. Collectively, these molecular features are compatible with roles in membrane-associated interactions, stress-related protein handling and EV-mediated intercellular communication, all of which are commonly associated with exosome biogenesis and secretion. In the context of TMZ treatment, these functions may contribute to tumour cell adaptation by maintaining protein homeostasis under chemotherapeutic stress and facilitating intercellular communication via exosomes, processes that have been implicated in chemoresistance.

Investigating the pathways in which these exosomal proteins participated provides a comprehensive view of their functions and predicts the underlying mechanisms involved in TMZ resistance (Figure 6b, Figure S8). Comparing with non-induced exosomes, KEGG enriched analysis demonstrated that the alterations of protein profiles in TMZ-induced exosomes (from 600 μg/mL TMZ condition) was predominantly enriched in the PI3K-Akt signalling pathway, a key intracellular pathway in regulating the cell cycle. In addition to PI3K-Akt signalling pathway, multiple KEGG pathways were also involved, such as endocrine, calcium reabsorption, thyroid hormone synthesis and ECM–receptor interaction. These pathways are commonly associated with cell survival signalling, calcium-dependent membrane dynamics, cytoskeletal remodelling and cell–matrix interactions, which overlap with endosomal trafficking and exosome biogenesis. Although several proteins were upregulated in TMZ-induced exosomes isolated from 100 and 300 μg/mL TMZ condition, KEGG enrichment analysis revealed that only efferocytosis pathway associated with apoptotic cell recognition was involved in 100 μg/mL TMZ condition, whereas no statistically significant enrichment in TMZ-induced exosomes isolated from 300 μg/mL TMZ condition. This may be attributed to functional heterogeneity of the upregulated proteins. Collectively, these results indicated a dose-dependent shift in the functional protein compositions and signal pathways of TMZ-induced exosomes, from efferocytosis-associated processes at lower TMZ concentrations to PI3K-Akt signalling pathways at higher TMZ concentrations. Furthermore, this shift may potentially reflect enhanced stress adaptation and anti-apoptotic action of tumour cells under high-dose chemotherapeutic stress. Meanwhile, these findings were also in line with above results that chemotherapy could increase production of exosomes, leading to enhanced cancer cell survival and resistance.

To identify the underlying DAPs interaction, we performed a protein–protein interaction (PPI) network revealing a cross reaction of MFGE8, HSP90AB1 and CFL1 with multiple proteins, indicating MFGE8, HSP90AB1 and CFL1 may be the major factors to drive the signalling pathways and biological functions (Figure 6c). Together, TMZ-induced exosomes exhibited upregulation of proteins involved in proteostasis, cell survival, phenotypic switching, metabolic adaption and exosome biogenesis, resulting in increased exosome secretion, which may further contribute to enhance TMZ resistance and therapeutic adaption. More importantly, the upregulated exosomal proteins may reflect a strategic mechanism that tumour cells tend to transfer resistance-associated exosomes to surrounding cells in the tumour microenvironment, thereby potentially enhancing the TMZ resistance of adjacent cells, which could well explain the reduced TMZ sensitivity of C6 cells after pretreatment with TMZ-induced exosomes.

4 | Discussion

TMZ serves as the first-line chemotherapeutic agent for GBM treatment; however, both intrinsic and acquired resistance significantly limit its therapeutic efficacy. Combinations of TMZ with various chemotherapy, immunotherapy and radiotherapy methods have been widely investigated in either preclinical studies or clinical settings to synergistically combat GBM (Chandran

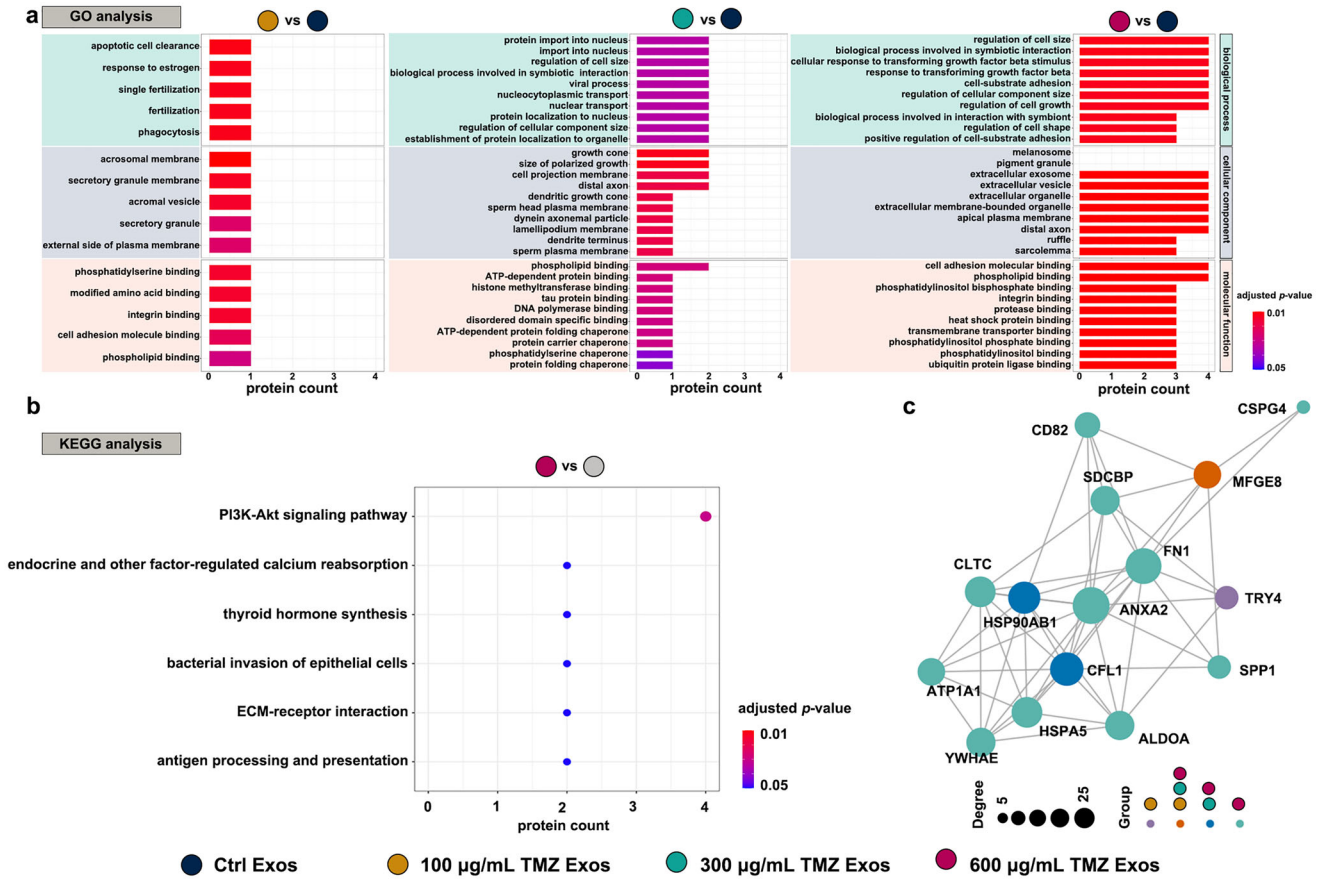

FIGURE 6 | TMZ-induced exosomes enriched in exosome biogenesis and chemoresistance related proteins. (a) GO analysis of biological process, cellular component and molecular function. The colour represents the significance of upregulating pathways. Colour ranges from blue to red, indicating higher levels of significance. (b) KEGG analysis of TMZ-induced exosomes compared with non-induced exosomes. Colour ranges from blue to red, indicating higher levels of significance. (c) Protein–protein interaction (PPI) network analysis of the relation of DAPs. *n* refers to independent biological experiments. DAP, differentially abundant protein; GO, Gene Ontology; KEGG, Kyoto Encyclopedia of Genes and Genomes; TMZ, temozolomide.

et al. 2017). Despite these approaches, the therapeutic efficacy of such combination therapies remains limited, highlighting the necessity for a deeper understanding of the mechanisms underlying TMZ resistance to improve GBM treatment outcomes. Increasing evidence indicates that tumour-derived exosomes play a critical role in angiogenesis, immune escape, invasion as well as therapeutic resistance through the transfer of proteins, nucleic acids and metabolites (Li and Nabet 2019). Although exosomes are increasingly recognised as mediators of chemoresistance, their specific role in TMZ resistance in GBM remains largely unclear. This study elucidates the relation between GBM-derived exosomes and TMZ resistance in GBM cells after exposure to TMZ, suggesting the therapeutic potential of targeting exosome biogenesis as a possible strategy to overcome TMZ resistance.

Based on the above findings, we attributed the upregulated protein profiles to TMZ-induced cellular stress, which may drive tumour cells to reprogram intracellular processes, leading to the enrichment of proteins associated with proteostasis, cell survival, phenotypic switching, metabolic adaption and exosome biogenesis. These reprogramed intracellular processes may reflect a self-protective and strategic mechanism by which tumour cells tend to better adapt to TMZ treatment, ultimately potentially contributing to the development of TMZ resistance. Moreover, the upregulated proteins may also enhance TMZ resistance in adjacent tumour cells after internalisation. In addition to promoting the TMZ resistance of adjacent tumour cells, exosomes may represent another possible mechanism associated with TMZ resistance by reducing intracellular drug accumulation through vesicular export from tumour cells. However, direct evidence for TMZ transport via exosomes is lacking due to its susceptibility to hydrolysis in vivo and moreover lacks intrinsic fluorescence, which raise the difficulty to detect prototype TMZ. Instead, we used DOX as alternative model drug given to its relatively stability and intrinsic fluorescence property (Ruan et al. 2015). According to the property of DOX, the content in exosomes derived from DOX-treated C6 cells was assessed. The results showed that DOX-induced exosomes approximately contained DOX at the concentration of 70 and 150 ng/mL after incubation for 24 and 48 h, demonstrating that exosomes can mediate drug export from drug-treated tumour cells (Figure S10). Importantly, given the substantial differences in physicochemical properties and stability between DOX and TMZ, the results had no direct evidence for TMZ incorporation into exosomes, but instead supported the possibility that chemotherapeutic agents may be exported via exosome-mediated pathways. Based on this, we speculated that TMZ may also be transported via exosomes, resulting in decreased intracellular TMZ accumulation and providing a potentially

mechanism underlying chemoresistance, which warrants further investigation. Furthermore, our hypothesis is supported by previous studies showing that exosomes can enhance the efflux of chemotherapeutic agents through multiple mechanisms, including directly exporting drugs via vesicular packing or indirectly facilitating drug efflux pathways, thereby reducing intracellular drug accumulation and potentially serve as a self-protecting and strategic mechanism underlying chemoresistance (Malla et al. 2025).

As aforementioned, the increased exosome secretion induced by TMZ is more likely attributed to the activation of p53-dependent secretory machinery. However, accumulating evidence indicates that autophagy, an intracellular degradation or self-protecting process, may also involve in exosome biogenesis, although this was not directly examined in the present study. Chemotherapeutic agents impose cell stress by inducing DNA damage, oxidative stress and metabolic perturbations, which in turn activate autophagy as an adaptive survival mechanism. During this process, LC3 (a ubiquitin-like protein) and other components of the autophagy machinery are recruited to autophagic membranes, facilitating the formation of autophagosomes and promoting intracellular homeostasis. These autophagosomes subsequently fuse with lysosomes to degrade and recycle cellular components, or fuse with cell membrane, an event that contributes to the cargo loading and consequent biogenesis of exosomes (Ma et al. 2023). Emerging evidence indicates that autophagy not only serves degradative functions but also intersects with exosome biogenesis pathways (Leidal et al. 2020). Specifically, stress-induced autophagy can enhance the formation of ILVs and MVBs, thereby promoting the exosome biogenesis and secretion (Fader and Colombo 2009). Based on these findings, we speculated that autophagy may also contribute to the increased exosome secretion observed under TMZ treatment; however, this possibility required direct experimental validation and thus remained an important direction for future investigation. Through this mechanism, tumour cells under chemotherapeutic stress may selectively package and export bioactive cargoes via exosomes, potentially including chemotherapeutic agents, which are subsequently transported into the extracellular environment.

As for treatment concentration of chemotherapeutics, TMZ (IC_{50} = 300 μg/mL), CDDP (IC_{50} = 200 μg/mL) and DOX (IC_{50} = 3 μg/mL) approximately the in vitro IC_{50} values for the GBM cells were selected rather than direct equivalents of clinical dosage (Yang et al. 2024). These concentrations enabled measurable cytotoxic stress and facilitated mechanistic evaluation of exosome secretion and cargo remodelling. It should be noted that these concentrations were substantially higher than those typically achieved in patients during standard clinical therapy. Given the existence of BBB and complexity of in vivo pharmacokinetics, the drug concentration at tumour site is generally much lower than the administration dose, even though TMZ is considered capable of penetrating the BBB. Therefore, the actual intracellular drug exposure could not be directly inferred from administered doses (Stern et al. 2010; Nichols et al. 2017). Moreover, the use of these concentrations provided a controlled framework to investigate how chemotherapeutic agents regulated exosome biogenesis and cargo composition, yielding qualitative mechanistic insights that may still be relevant under physiological conditions. Future studies using clinically relevant dosage or in vivo models will be crucial to validate and extend these findings.

In summary, our findings identify exosome biogenesis as a previously underappreciated adaptive response to TMZ-induced stress in GBM cells. Through activation of p53-STEAP3-dependent secretory machinery, TMZ enhances exosome biogenesis without altering their integrity, physiochemical property, and biological identity, enabling efficient intercellular communication within the tumour environment. The ability of TMZ-induced exosomes to reduce apoptosis and attenuate TMZ sensitivity that they may play a contributory role in driving chemoresistance, providing a potential explanation for the limited survival benefit of TMZ. However, although protein components have been suggested to contribute to the observed effect, it remains unclear whether additional exosomal factors are also involved. The current study does not exclude potential contributions from other cargo, such as RNAs, lipids or surface molecules. Accordingly, TMZ-induced exosome may represent a potential chemoresistance-associated mechanism, which is only validated in cellular level, further in vivo studies are required to validate the role of exosomes in mediating chemoresistance and to explore their potential as therapeutic targets for overcoming resistance. Overall, this study offers a new insight for improving therapeutic efficacy of TMZ as well as the survival benefit in GBM patients.

Author Contributions

Wenpei Li: methodology, formal analysis, investigation, writing – original draft. **Shaoping Jiang**: methodology, formal analysis. **Kun Liu**: proteomics analysis. **Zhi Li**: methodology. **Jun Yang**: methodology. **Weimin Liu**: methodology. **Yuanyu Huang**: writing – review, supervision, funding acquisition. **Minghui Yang**: methodology, formal analysis. **Shuai Guo**: writing – review, funding acquisition. **Shaobo Ruan**: conceptualisation, methodology, formal analysis, writing – original draft, writing – review and editing, funding acquisition, supervision.

Acknowledgements

We thank the Biological and Medical Engineering Core Facilities, and Analysis and Testing Center, Beijing Institute of Technology for supporting experimental equipment and staff for valuable help with technical support. We also thank Quantum Scientific Instruments Trading (Beijing) Co., Ltd for their supporting with NanoView. We also like to thank Beijing De quan xing ye Commerce & Trade Co., Ltd. for providing the CytoFLEX nano equipment. We thank Can Huang, Engineer Qianwen Li and Engineer Yufei Wang for providing technical support with the CytoFLEX nano Flow cytometer and NanoView.

Funding

This work received funding from National Natural Science Foundation of China grant 22575024 and 82302387 (S.R.), Beijing Natural Science Foundation grant L222128 (S.R.) and 7264406 (S.G.), Beijing Municipal Science & Technology Commission Medical Innovation Products and Platform Cultivation Fund Z241100009024001 (Y.H.) and Beijing Institute of Technology Research Fund Program for Young Scholars grant XSQD-202121010 (S.R.).

Conflicts of Interest

The authors declare no conflicts of interest.

Data Availability Statement

All data needed to evaluate the conclusions in the paper are present in the paper and/or the Supplementary Materials.

References

Arya, S. B., S. P. Collie, and C. A. Parent. 2024. "The Ins-and-Outs of Exosome Biogenesis, Secretion, and Internalization." *Trends in Cell Biology* 34, no. 2: 90–108.

Babi, A., K. Menlibayeva, T. Bex, et al. 2022. "Targeting Heat Shock Proteins in Malignant Brain Tumors: From Basic Research to Clinical Trials." *Cancers* 14, no. 21: 5435.

Berenguer, J., T. Lagerweij, X. W. Zhao, et al. 2018. "Glycosylated Extracellular Vesicles Released by Glioblastoma Cells Are Decorated by CCL18 Allowing for Cellular Uptake via Chemokine Receptor CCR8." *Journal of Extracellular Vesicles* 7, no. 1: 1446660.

Broekman, M. L., S. L. N. Maas, E. R. Abels, et al. 2018. "Multidimensional Communication in the Microenvirons of Glioblastoma." *Nature Reviews Neurology* 14, no. 8: 482–495.

Brosseau, C., L. Colas, A. Magnan, et al. 2018. "CD9 Tetraspanin: A New Pathway for the Regulation of Inflammation?" *Frontiers in Immunology* 9: 2316.

Chandran, M., M. Candolfi, D. Shah, et al. 2017. "Single Vs. Combination Immunotherapeutic Strategies for Glioma." *Expert Opinion on Biological Therapy* 17, no. 5: 543–554.

Chen, Y., Y. Jin, and N. Wu. 2021. "Role of Tumor-Derived Extracellular Vesicles in Glioblastoma." *Cells* 10, no. 3: 512.

Cheng, H. Y., C. H. Hsieh, P. H. Lin, et al. 2022. "Snail-Regulated Exosomal microRNA-21 Suppresses NLRP3 Inflammasome Activity to Enhance Cisplatin Resistance." *Journal for ImmunoTherapy of Cancer* 10, no. 8: e004832.

Das, A., P. Saha, K. Kalele, et al. 2024. "Clinical Signature of Exosomal Tetraspanin Proteins in Cancer." *Clinical and Translational Discovery* 4, no. 4: e341.

Deng, Y., Z. Chen, P. Chen, et al. 2025. "ALKBH3-Regulated m1A of ALDOA Potentiates Glycolysis and Doxorubicin Resistance of Triple Negative Breast Cancer Cells." *Acta Pharmaceutica Sinica B* 15, no. 6: 3092–3106.

Dusoswa, S. A., S. K. Horrevorts, M. Ambrosini, et al. 2019. "Glycan Modification of Glioblastoma-Derived Extracellular Vesicles Enhances Receptor-Mediated Targeting of Dendritic Cells." *Journal of Extracellular Vesicles* 8, no. 1: 1648995.

Eun, J. W., J. H. Yoon, H. R. Ahn, et al. 2023. "Cancer-Associated Fibroblast-Derived Secreted Phosphoprotein 1 Contributes to Resistance of Hepatocellular Carcinoma to Sorafenib and Lenvatinib." *Cancer Communications* 43, no. 4: 455–479.

Fader, C. M., and M. I. Colombo. 2009. "Autophagy and Multivesicular Bodies: Two Closely Related Partners." *Cell Death and Differentiation* 16, no. 1: 70–78.

Fan, Y., Z. Gao, J. Xu, et al. 2023. "SPI1-Mediated MIR222HG Transcription Promotes Proneural-to-Mesenchymal Transition of Glioma Stem Cells and Immunosuppressive Polarization of Macrophages." *Theranostics* 13, no. 10: 3310–3329.

Fu, R., Q. Shen, P. Xu, et al. 2014. "Phagocytosis of Microglia in the Central Nervous System Diseases." *Molecular Neurobiology* 49, no. 3: 1422–1434.

Ghossoub, R., F. Lembo, A. Rubio, et al. 2014. "Syntenin-ALIX Exosome Biogenesis and Budding into Multivesicular Bodies Are Controlled by ARF6 and PLD2." *Nature Communications* 5, no. 1: 3477.

Gurung, S., D. Perocheau, L. Touramanidou, et al. 2021. "The Exosome Journey: From Biogenesis to Uptake and Intracellular Signalling." *Cell Communication and Signaling* 19, no. 1: 47.

Han, B., X. Meng, P. Wu, et al. 2020. "ATRX/EZH2 Complex Epigenetically Regulates FADD/PARP1 Axis, Contributing to TMZ Resistance in Glioma." *Theranostics* 10, no. 7: 3351–3365.

Han, Q. F., W. J. Li, K. S. Hu, et al. 2022. "Exosome Biogenesis: Machinery, Regulation, and Therapeutic Implications in Cancer." *Molecular Cancer* 21, no. 1: 207.

Hu, Q., J. Yao, X. Wu, et al. 2022. "Emodin Attenuates Severe Acute Pancreatitis-Associated Acute Lung Injury by Suppressing Pancreatic Exosome-Mediated Alveolar Macrophage Activation." *Acta Pharmaceutica Sinica B* 12, no. 10: 3986–4003.

Hussain, M. T., S. Austin-Williams, J. McCay, et al. 2025. "Comparative Assessment of Whole Organ Tissue Processing Methods for the Isolation of Extracellular Vesicles From Intact Organs." *Journal of Extracellular Vesicles* 14, no. 9: e70127.

Jankovičová, J., P. Sečová, K. Michalková, et al. 2020. "Tetraspanins, More than Markers of Extracellular Vesicles in Reproduction." *International Journal of Molecular Sciences* 21, no. 20: 7568.

Jiang, S., W. Li, J. Yang, et al. 2024. "Cathepsin B-Responsive Programmed Brain Targeted Delivery System for Chemo-Immunotherapy Combination Therapy of Glioblastoma." *ACS Nano* 18, no. 8: 6445–6462.

Kimiz-Gebologlu, I., and S. S. Oncel. 2022. "Exosomes: Large-Scale Production, Isolation, Drug Loading Efficiency, and Biodistribution and Uptake." *Journal of Controlled Release* 347: 533–543.

Lee, S. Y. 2016. "Temozolomide Resistance in Glioblastoma Multiforme." *Genes & Diseases* 3, no. 3: 198–210.

Lee, Y. J., K. J. Shin, and Y. C. Chae. 2024. "Regulation of Cargo Selection in Exosome Biogenesis and Its Biomedical Applications in Cancer." *Experimental & Molecular Medicine* 56, no. 4: 877–889.

Leidal, A. M., H. H. Huang, T. Marsh, et al. 2020. "The LC3-Conjugation Machinery Specifies the Loading of RNA-Binding Proteins into Extracellular Vesicles." *Nature Cell Biology* 22, no. 2: 187–199.

Lespagnol, A., D. Duflaut, C. Beekman, et al. 2008. "Exosome Secretion, Including the DNA Damage-Induced p53-Dependent Secretory Pathway, Is Severely Compromised in TSAP6/Steap3-Null Mice." *Cell Death and Differentiation* 15, no. 11: 1723–1733.

Li, G., Z. Xiong, Y. Li, et al. 2024. "Hypoxic Microenvironment-Induced Exosomes Confer Temozolomide Resistance in Glioma Through Transfer of Pyruvate Kinase M2." *Discover Oncology* 15, no. 1: 110.

Li, I., and B. Y. Nabet. 2019. "Exosomes in the Tumor Microenvironment as Mediators of Cancer Therapy Resistance." *Molecular Cancer* 18, no. 1: 32.

Li, P., M. Kaslan, S. H. Lee, et al. 2017. "Progress in Exosome Isolation Techniques." *Theranostics* 7, no. 3: 789–804.

Li, Z., X. Meng, P. Wu, et al. 2021. "Glioblastoma Cell-Derived lncRNA-Containing Exosomes Induce Microglia to Produce Complement C5, Promoting Chemotherapy Resistance." *Cancer Immunology Research* 9, no. 12: 1383–1399.

Liang, Y., L. Duan, J. Lu, et al. 2021. "Engineering Exosomes for Targeted Drug Delivery." *Theranostics* 11, no. 7: 3183–3195.

Liu, C., J. Zhao, F. Tian, et al. 2019. "Low-Cost Thermophoretic Profiling of Extracellular-Vesicle Surface Proteins for the Early Detection and Classification of Cancers." *Nature Biomedical Engineering* 3, no. 3: 183–193.

Ma, Y., L. Sun, J. Zhang, et al. 2023. "Exosomal mRNAs for Angiogenic–Osteogenic Coupled Bone Repair." *Advanced Science* 10, no. 33: e2302622.

Ma, Z., Y. Sun, Y. Yu, et al. 2024. "Extracellular Vesicles Containing MFGE8 From Colorectal Cancer Facilitate Macrophage Efferocytosis." *Cell Communication and Signaling* 22, no. 1: 295.

Malla, R., P. Bhamidipati, A. S. Samudrala, et al. 2025. "Exosome-Mediated Cellular Communication in the Tumor Microenvironment Imparts Drug Resistance in Breast Cancer." *Cancers (Basel)* 17, no. 7: 1167.

Munoz, J. L., N. D. Walker, K. W. Scotto, et al. 2015. "Temozolomide Competes for P-Glycoprotein and Contributes to Chemoresistance in Glioblastoma Cells." *Cancer Letters* 367, no. 1: 69–75.

Naumann, S. C., W. P. Roos, E. Jöst, et al. 2009. "Temozolomide-and Fotemustine-Induced Apoptosis in Human Malignant Melanoma Cells: Response Related to MGMT, MMR, DSBs, and p53." *British Journal of Cancer* 100, no. 2: 322–333.

Nehrbas, J., J. T. Butler, D. W. Chen, et al. 2020. "Extracellular Vesicles and Chemotherapy Resistance in the AML Microenvironment." *Frontiers in Oncology* 10: 90.

Nichols, J. W., Y. Sakurai, H. Harashima, et al. 2017. "Nano-Sized Drug Carriers: Extravasation, Intratumoral Distribution, and Their Modeling." *Journal of Controlled Release* 267: 31–46.

Oldrini, B., N. Vaquero-Siguero, Q. Mu, et al. 2020. "MGMT Genomic Rearrangements Contribute to Chemotherapy Resistance in Gliomas." *Nature Communications* 11, no. 1: 3883.

Qin, T. Q., Y. Qin, H. Wen, et al. 2025. "Hypoxic Neural Stem Cells Enhance Spinal Cord Repair Through HIF-1a/RAB17-Driven Extracellular Vesicle Release." *Journal of Extracellular Vesicles* 14, no. 7: e70126.

Robey, R. W., K. M. Pluchino, M. D. Hall, et al. 2018. "Revisiting the Role of ABC Transporters in Multidrug-Resistant Cancer." *Nature Reviews Cancer* 18, no. 7: 452–464.

Ruan, S., M. Yuan, L. Zhang, et al. 2015. "Tumor Microenvironment Sensitive Doxorubicin Delivery and Release to Glioma Using Angiopep-2 Decorated Gold Nanoparticles." *Biomaterials* 37: 425–435.

Simon, T., E. Jackson, and G. Giamas. 2020. "Breaking Through the Glioblastoma Micro-environment via Extracellular Vesicles." *Oncogene* 39, no. 23: 4477–4490.

Song, J., D. Zhao, G. Sun, et al. 2021. "PTPRM Methylation Induced by FN1 Promotes the Development of Glioblastoma by Activating STAT3 Signalling." *Pharmaceutical Biology* 59, no. 1: 902–909.

Song, X.., Y. Song, J. Zhang, et al. 2024. "Regulatory Role of Exosome-Derived miRNAs and Other Contents in Adipogenesis." *Experimental Cell Research* 441, no. 1: 114168.

Soumoy, L., A. Genbauffe, L. Mouchart, et al. 2024. "ATP1A1 Is a Promising New Target for Melanoma Treatment and Can Be Inhibited by Its Physiological Ligand Bufalin to Restore Targeted Therapy Efficacy." *Cancer Cell International* 24, no. 1: 8.

Stern, S. T., J. B. Hall, L. L. Yu, et al. 2010. "Translational Considerations for Cancer Nanomedicine." *Journal of Controlled Release* 146, no. 2: 164–174.

Tso, J. L., S. Yang, J. C. Menjivar, et al. 2015. "Bone Morphogenetic Protein 7 Sensitizes O6-Methylguanine Methyltransferase Expressing-Glioblastoma Stem Cells to Clinically Relevant Dose of Temozolomide." *Molecular Cancer* 14, no. 1: 189.

Wan, M., B. Ning, S. Spiegel, et al. 2019. "Tumor-Derived Exosomes (TDEs): How to Avoid the Sting in the Tail." *Medicinal Research Reviews* 40, no. 1: 385–412.

Wang, L., X. Tian, R. Gyawali, et al. 2013. "Fungal Adhesion Protein Guides Community Behaviors and Autoinduction in a Paracrine Manner." *Proceedings of the National Academy of Sciences of the United States of America* 110, no. 28: 11571–11576.

Wang, L. L., J. Luo, Z. H. He, et al. 2021. "STEAP3 Promotes Cancer Cell Proliferation by Facilitating Nuclear Trafficking of EGFR to Enhance RAC1-ERK-STAT3 Signaling in Hepatocellular Carcinoma." *Cell Death & Disease* 12, no. 11: 1052.

Wang, T., Z. Wang, R. Niu, et al. 2019. "Crucial Role of Anxa2 in Cancer Progression: Highlights on Its Novel Regulatory Mechanism." *Cancer Biology & Medicine* 16, no. 4: 671–687.

Wong, B. S., S. R. Shah, C. L. Yankaskas, et al. 2020. "A Microfluidic Cell-Migration Assay for the Prediction of Progression-Free Survival and Recurrence Time of Patients With Glioblastoma." *Nature Biomedical Engineering* 5, no. 1: 26–40.

Wu, J., H. Yang, J. Cheng, et al. 2020. "Knockdown of Milk-Fat Globule EGF Factor-8 Suppresses Glioma Progression in GL261 Glioma Cells by Repressing Microglial M2 Polarization." *Journal of Cellular Physiology* 235, no. 11: 8679–8690.

Wu, P., J. Cai, Q. Chen, et al. 2019. "Lnc-TALC Promotes O6-Methylguanine-DNA Methyltransferase Expression via Regulating the c-Met Pathway by Competitively Binding With miR-20b-3p." *Nature Communications* 10, no. 1: 2045.

Wu, S., X. Li, F. Gao, et al. 2021. "PARP-Mediated PARylation of MGMT Is Critical to Promote Repair of Temozolomide-Induced O6-Methylguanine DNA Damage in Glioblastoma." *Neuro-Oncology* 23, no. 6: 920–931.

Xia, B., Y. Liu, J. Wang, et al. 2023. "Emerging Role of Exosome-Shuttled Noncoding RNAs in Gastrointestinal Cancers: From Intercellular Crosstalk to Clinical Utility." *Pharmacological Research* 195: 106880.

Xie, S., Q. Zhang, and L. Jiang. 2022. "Current Knowledge on Exosome Biogenesis, Cargo-Sorting Mechanism and Therapeutic Implications." *Membranes* 12, no. 5: 498.

Xiong, Q., B. Yin, H. Jiang, et al. 2025. "Targeting CSPG4 Enhances the Anti-Tumor Activity of CAR-NK Cells for Glioblastoma." *Cellular Oncology (Dordrecht)* 48, no. 5: 1539–1551.

Xu, J., Y. Guo, W. Ning, et al. 2025. "Comprehensive Analysis of Heat Shock Proteins in Glioma Revealed the Association with Glioma-Associated Myeloid Cells." *Genes & Immunity* 26, no. 3: 200–212.

Xu, X., Y. Zheng, L. Luo, et al. 2024. "Glioblastoma Stem Cells Deliver ABCB4 Transcribed by ATF3 via Exosomes Conferring Glioblastoma Resistance to Temozolomide." *Cell Death & Disease* 15, no. 5: 318.

Yadav, A., A. Nandy, A. Sharma, et al. 2024. "Exosome Mediated Cell-Cell Crosstalk in Tissue Injury and Repair." *Intercellular and Interorganellar Transfer and Communication in Biology and Medicine* 73: 249–297.

Yang, E., X. Wang, Z. Gong, et al. 2020. "Exosome-Mediated Metabolic Reprogramming: The Emerging Role in Tumor Microenvironment Remodeling and Its Influence on Cancer Progression." *Signal Transduction and Targeted Therapy* 5, no. 1: 242.

Yang, J., Y. Li, S. Jiang, et al. 2024. "Engineered Brain-Targeting Exosome for Reprogramming Immunosuppressive Microenvironment of Glioblastoma." *Exploration* 5, no. 2: 20240039.

Yin, J., X. Wang, X. Ge, et al. 2023. "Hypoxanthine Phosphoribosyl Transferase 1 Metabolizes Temozolomide to Activate AMPK for Driving Chemoresistance of Glioblastomas." *Nature Communications* 14, no. 1: 5913.

Yin, J., A. Zeng, Z. Zhang, et al. 2019. "Exosomal Transfer of miR-1238 Contributes to Temozolomide-Resistance in Glioblastoma." *eBioMedicine* 42: 238–251.

Yu, D.., Y. Li, M. Wang, et al. 2022. "Exosomes as a New Frontier of Cancer Liquid Biopsy." *Molecular Cancer* 21, no. 1: 56.

Zhang, S., S. J. Chuah, R. C. Lai, et al. 2018. "MSC Exosomes Mediate Cartilage Repair by Enhancing Proliferation, Attenuating Apoptosis and Modulating Immune Reactivity." *Biomaterials* 156: 16–27.

Supporting Information

Additional supporting information can be found online in the Supporting Information section.

Supporting Information: jex270161-sup-0001-FigureS1-S10.docx